Journal of Materials Chemistry A

Three-Dimensional SWCNT and MWCNT Hybrid Networks for Extremely High-loading and High Rate Cathode Materials

Journal:	*Journal of Materials Chemistry A*
Manuscript ID	TA-ART-04-2019-003870.R2
Article Type:	Paper
Date Submitted by the Author:	24-Jun-2019
Complete List of Authors:	Kim, Dae-wook; Shinshu University, Department of Materials Chemistry Zettsu, Nobuyuki; Shinshu University Faculty of Engineering, Department of Materials Chemistry; Shinshu University, Research Initiative for Supra-Materials Teshima, Katsuya; Shinshu University, Research Initiative for Supra-Materials; Shinshu University Faculty of Engineering, Department of Materials Chemistry

Journal Name

ARTICLE

Three-Dimensional SWCNT and MWCNT Hybrid Networks for Extremely High-loading and High Rate Cathode Materials

Dae-wook Kim,[a] Nobuyuki Zettsu*[ab] and Katsuya Teshima*[ab]

Received 00th January 20xx,
Accepted 00th January 20xx

DOI: 10.1039/x0xx00000x

www.rsc.org/

Extremely high-loading $LiNi_{0.5}Co_{0.2}Mn_{0.3}O_2$ (NCM523) cathode materials (up to 99.5 wt%) were achieved through self-organization of a three-dimensional network of multi-walled and single-walled CNT hybrids. The full cell using the NCM523 cathode/graphite without any conventionally used insulating binder exhibited superior C-rate capability (105 mAh/g at 10 C) and remarkably improved cycling stability (94% capacity after 300 cycles at 1 C). The hybridization of a small amount of single-walled CNTs enabled a fast lithiation/delithiation reaction with less polarization and prevented intergranular cracking in both the individual NCM523 secondary particles and NCM523 electrodes during cycling.

1. Introduction

To cope with climate change, leading industrial countries have made great efforts to strengthen the regulation of warming gas and gas mileage for automobiles. With the increasing demands and rapid expansion of the green vehicle technologies, automobiles are shifting from internal combustion to electrical conversion engines. There are many candidates for electrical conversion systems, including fuel cell and Li-ion, Ni metal hydride, and lead-acid batteries. Among these, Li-ion batteries are the most attractive candidates owing to their higher energy density and lower hysteresis.[1–4] However, they have many limitations such as the need for higher energy density of over ca. 700 Wh/L (corresponding gravimetric energy density is ca. 300 Wh/kg) while maintaining long-term stability (100,000 miles for 8 years) and safety issues.[5–8] The battery community has found it generally difficult to handle paradoxical issues (energy density and stability) simultaneously. To overcome these technical difficulties from the perspective of cathode, researchers have devoted much effort to investigating high-specific capacity materials such as Li or Ni-rich layered oxides ($LiNi_{1-x-y}Co_xMn_yO_2$, NCM; $LiNi_{1-x-y}Co_xAl_yO_2$, NCA).[9–13] Owing to their efforts involving experimental and theoretical approaches, many surprising progresses have been achieved such as a high reversible specific capacity of over 220 $mAh{\cdot}g^{-1}$.

Other approaches from the perspective of peripheral components are essential to further improve the battery performances. For instance, increasing the loading of active materials with the elimination of both electrically conducting carbon and insulating polymeric binders could be another way of improving the energy density. Since Kuwabata and colleagues first reported the use of polypyrrole as a coating material on a spinel $LiMn_2O_4$ electrode, conjugated polymers have been extensively studied as electrode coating materials for energy storage devices because their tunable doping permits engineering of the ionic and electronic transport properties.[14,15] The electrochemically doped poly(3-hexylthiophene-2,5-diyl) provided high electronic and ionic conductivity and led to the mitigation of degradation due to side reactions driven by the transition metal dissolution, formation of a thick solid electrolyte interface (SEI), and intergranular cracking in $LiNi_{0.82}Co_{0.15}Al_{0.03}O_2$ secondary particles.[16]

Multi-walled carbon nanotubes (MWCNTs) having much higher conductivity than that of conjugating polymers are attractive materials as electron conductive agents as well as electron conducting binders to replace conventionally used carbon black and insulating polymeric binders. Such replacement enabled to increase the loading amount of active materials in the composite electrodes, maintaining enough Li+ accessibility inside the electrode, which simultaneously enhanced their C-rate capability and cyclability.[17–19] However, the elimination of polymeric binders imposed a limitation in the loading amount of active materials and further generated harmful effects on the binding stiffness of the electrode with the current collector. Since CNTs distribute randomly in the electrodes, they tend to cause severe micro-cracks at the electrode/current collector interface during long cycle operations.

Based on these backgrounds, we demonstrate three-dimensional (3D) electric micro-grid network structures as one of the ideal electrode systems to further improve the energy density with enough adhesion for long cycle operations.[20]

[a] Department of Materials Chemistry, Faculty of Engineering, Shinshu University, 4-17-1 Wakasato, Nagano 380-8553, Japan. E-mail: teshima@shinshu-u.ac.jp and zettsu@shinshu-u.ac.jp
[b] Research Initiative for Supra-Materials, Shinshu University, 4-17-1 Wakasato, Nagano 380-8553, Japan.

† Electronic Supplementary Information (ESI) available: Morphology of NCM/ and NCA/SW electrodes. Interfacial resistivity of NCM/SW electrodes. CV curves and EIS parameter of NCM/SW half-cell. See DOI: 10.1039/x0xx00000x

Supramolecular assemblies of $LiNi_{0.5}Co_{0.2}Mn_{0.3}O_2$ (NCM523) and MWCNT electrodes enabled to increase the NCM523 loading up to 98 wt% and the tap density up to 3.8 $g \cdot cm^{-3}$ by eliminating the need for a PVDF binder. Furthermore, higher C-rate capability and cyclability were achieved by improving the kinetic parameters of the battery reactions. Since the supramolecular assemblies can be prepared using a conventional NMP-based slurry coating, they would provide high flexibility for mass production. However, the MWCNT-based 3D network showed limitations in both kinetic parameters and robustness of the electrodes. The increase in the loading of active materials to more than 99 wt% weakened the binding force and lowered the electron conductivity, leading to inhibition of Li+ accessibility inside the electrode. Furthermore, it rendered the fabricated electrode unstable.

Herein, we propose a 3D network of hybrid MWCNT and SWCNT assembly to achieve an extremely high-loading NCM523 cathode having a loading of over 99.5 wt% to further improve the energy density to more than 700 $Wh \cdot L^{-1}$.

2. Experimental section

2.1 Preparation of NCM/CNTs electrodes

Commercially available active materials (NCM523, NCA) and multi walled CNTs (MWCNTs) and single walled CNTs (SWCNTs) solutions were used for the preparation of the all electrodes with 3D hybrid network structures. The concentration of CNTs were 9 wt% and 0.2 wt% for MWCNTs and SWCNTs, respectively. The length of CNTs is ca. 500 nm (MWCNTs) and 5~10 μm (SWCNTs), as analyzed by SEM observation (Fig. S1). The mixtures of active materials and CNTs solutions were prepared by using a planetary centrifugal mixer (THINNKY MIXER AR-100). The mixture was homogeneously coated on a 15 μm thick Al sheet as a current collector by using a Baker-type applicator with controlled coating speed. The loading amount of NCM523 particles was adjusted to ca. 6.5 mg/cm^2. The thickness of the electrode was averagely 37 μm, as evaluated by cross-sectional FE-SEM observation. The obtained electrodes were dried in a vacuum oven for 1 day. The ratio of active materials was adjusted to 99 or 99.5 wt%. The ratio of SWCNTs for total amount of CNTs were adjusted to 0 ~ 15 %. The all prepared electrodes compositions were summarized in the Table S1. The electrodes were pressed to be controlled their tap density of ca. 3.0 g/cc.

2.2 Characterization

The microstructures of prepared electrodes were observed by field emission scanning electron microscopy (FE-SEM, JEOL, JSM7600F at 5 kV). The phase transition of the cycled electrodes was examined using X-ray diffraction (XRD) analysis with a Cu-Kα radiation source (Miniflex II; Rigaku). It was operated at 30 kV and 20 mA, with 2θ = 10–80°. The electrical conductivity and interfacial resistivity of electrodes was examined by using a multi-point probe system (XF057, Hioki). In order to examine electrochemical characteristics for prepared electrodes, a coin-type R2032 cell was used, and the coin cells were prepared in the Ar-filled glovebox (MIWA MFG Co. Ltd). For the half-cell assembling, a lithium foil (14 mm in dia.) and a polypropylene film (Celgard #2500) were used as a counter electrode and a separator, respectively. One molarity (1M) of $LiPF_6$ in a mixture of ethylene carbonate and dimethyl carbonate (3 : 7, v/v) was used as an electrolyte. In case of the full-cell assembling, graphite electrode, kindly supplied from Maxell Holdings, Ltd., was used as anode electrode. 0.5 wt% of vinylene carbonate was added in the electrolyte. The galvanostatic charge–discharge tests were conducted between 2.8 and 4.3 V (V vs. Li/Li^+) using a battery test unit (Hokuto Denko, HJ1020Msd8). The cyclic voltammetry (CV) curves were conducted between 2.8 and 4.4 V (V vs. Li/Li^+) at the various scan rate from 0.1 to 1.5 mV/s using electrochemical workstation (Biologic, VSP-300). The electrochemical impedance spectroscopy (EIS) measurements were performed in the frequency range between 200 kHz and 1 mHz by using electrochemical workstation (Biologic, VSP- 300). All electrochemical measurements were performed in a constant temperature chamber (Espec, SU-221) at room temperature.

3. Results and discussion

3.1 Microstructure of 3D network system

The supramolecular NCM523/MWCNT/SWCNT assembled electrodes with different architectures were prepared from a NMP-based slurry. The concentration of NCM523 particles were controlled between 99 and 99.5 wt%. The remaining 1–0.5 wt% was composed of a mixture of MWCNT and SWCNT at a designated weight ratio. For convenience, the prepared electrodes were denoted as 99NCM/SW0, 995NCM/SW0, 995NCM/SW10, 995NCM/SW12, and 995NCM/SW15. The detailed procedures are provided in the supporting information.

The microstructure of NCM523 in the CNT composites was examined by FE-SEM. The composite electrodes showed different morphologies, depending on the presence of SWCNTs (Fig. 1 and S2). First, 99NCM/SW0 and 995NCM/SW0 are compared in detail. The high-magnification SEM images show that the MWCNTs in the 99NCM/SW0 electrode are homogeneously distributed over the NCM523 particle surface. Each secondary NCM523 particle is closely bridged by the CNT hybrid, leading to the formation of a micro-grid network in the electrodes. In contrast, the MWCNT network in the 995NCM/SW0 electrode is formed mostly at the grain boundary of each NCM523 primary particle. This difference in microstructure occurred due to the lack of sufficient MWCNTs required to cover the entire surface and the affinity of the MWCNTs. The MWCNTs preferentially aggregated at the grain boundaries and formed nanospaces between the neighbouring particles than on the particle surface. This suggests that MWCNTs preferentially disperse in the NMP solution to become energetically stable rather than adsorbing on the NCM523 particle surface (Fig. S2 and Fig. 1c). The SWCNTs were further added as a second CNTs candidates since its light weight and longer length and higher electron conductivity, as comparing to

that of MW-CNT used here. We expect increasing a number of SWCNTs stands expand coverage and makes up for the lack of electron conductivity of MW-CNTs while maintaining the 3D network structure. The hybridization with SWCNTs resulted in significant morphological changes. As shown in Fig. 1d–f, longer SWCNTs (5–10 μm) homogeneously dispersed on the secondary NMC523 particle surface and densely bridged the neighbouring particles in the 995NCM/SW12 electrode. These observations indicated that the short MWCNTs (ca. 500 nm) were primarily consumed in the formation of the junction at the grain boundary as well as the intergranular nanospaces, whereas the SWCNTs adsorbed on the surface and grain boundary due to their length and stretchability. The shear force acting on the NMP paste in the coating process caused the elongation of SWCNTs, making it difficult for the SWCNTs to enter the grain boundary. A plausible formation mechanism of the 3D network structure is schematically illustrated in Fig. 1g.

3.2 Electrochemical properties of NCM/SW electrodes

The hybridization of MWCNT and SWCNT networks increased the electrical conductivity and accessibility during the charging-discharging reactions resulting in high cyclability, even though polymeric binders did not assist the highly loaded NCM523 electrodes. As shown in the galvanostatic charge–discharge profiles obtained at a current density of 33 mA/g corresponding to 0.2 C (Fig. 2a), all the prepared electrodes presented a discharge capacity of approximately 170 mAh/g without any significant difference in the given test conditions. Specific capacity is represented in terms of weight of the NCM523 particles; this suggests that the hybridized 3D network provided an ideal charge-discharge reaction with no capacity fading and overpotential due to the internal resistance of the cell. Meanwhile, their C-rate capabilities were different, depending on the SWCNT content (Fig. 2b). Compared with the 99NCM/SW0 electrode, the 995NCM/SW0 electrode showed gradual degradation with increasing current density. The discharge capacity decreased to 62 mAh/g at 10 C; such a remarkable capacity fading can be explained by different microstructural characteristics depending on the CNT content, as discussed in Fig. 1. The lack of CNT networks required for fully covering the NCM523 primary particle surfaces appeared to contribute to poor kinetics via disconnection of electron conduction networks, leading to the degradation of C-rate capability. Further, the 99NCM/SW0 electrode presented a comparable rate capability to those of 995NCM/SW10 and 995NCM/SW15 electrodes. These results clearly demonstrated that 1 wt% of MWCNTs is the minimum requirement for the formation of 3D networks with full coverage of the NCM523 electrodes without performance degradation. Interestingly, with a further increase in NCM523 loading up to 99.5 wt%, the SWCNTs became essential for connecting the electrical pathways by covering all the individual NCM523 primary particle surfaces, which would counteract the lack of total CNT content. Moreover, the hybridization of SWCNTs and MWCNTs is a critical factor for constructing a 3D network providing higher C-rate capability. Due to successful hybridization, 995NCM/SW12 presented a much smaller capacity loss with an increase in current density, compared with the 99NCM/SW0 electrode. Furthermore, the discharge capacity of 105 mAh/g at 10 C is significantly superior to those previously reported.[20–25] It is considered that the 995NCM/SW12 electrode achieves accessibility to the electrolyte, which is strongly related to the facilitation of Li-ion migration.

Cyclic voltammetry (CV) was performed to determine the effect of hybridization on the electrochemical polarization and kinetics. We compared the kinetics during lithiation/delithiation reactions in the half-cells (Fig. 2c). The 995NCM/SW0 electrode showed the lowest current density with broad peaks and larger separation between the anodic and cathodic peaks. In contrast, sharp peaks with a flat plateau and smaller peak separation were observed in the 99NCM/SW0 and 995NCM/SWs electrodes. This implies that the hybridized CNT 3D network supports fast lithiation/delithiation reaction with less polarization.[26,27] The calculated diffusion coefficient of Li ions (D_{Li}) indicated the effect of different material composition (Fig. 2d, Fig. S3, and Table S2). D_{Li} was calculated from both anodic and cathodic currents at higher scan rates from 0.1 to 1.5 mV/s. The 995NCM/SW12 electrode resulted in the highest D_{Li} in both lithiation/delithiation reactions. An obvious impact was recognized in the delithiation process, *i.e.*, the 995NCM/SW12 electrode would be greatly effective in fast charging of the battery. These results are in good agreement with the battery performance and explain the improved C-rate capability.

The electrical conductivity of the NCM/SWs electrodes shown in Fig. 2e was measured using a multi-probe system. 99NCM/SW0 showed higher conductivity than that of 995NCM/SW0 due to the formation of a robust electronic pathway comprising surplus CNTs. It is noteworthy that 995NCM/SW12 showed comparable electrical conductivity to that of 99NCM/SW0, even though the loading amount of conductive carbon was half of that of the 99NCM/SW0 electrode. Similarly, numerically analysed interfacial resistivity between the current collector and composite layers showed that 995NCM/SW0 had the highest resistance among all the prepared electrodes (Table S3). This implies that insufficient contact between the current collector and composite layers mitigates electron transfer, which negatively affects the battery performance. Moreover, the 995NCM/SW12 electrode presented slightly lower surface (R_{sf}) and charge transfer (R_{CT}) resistances (Fig. 2f and Table S4), as evaluated by electrochemical impedance spectroscopy. These results represented consistent trends within the series of NCM/SW electrode systems. The variation in electrochemical properties with the SWCNT content suggested that excessive SWCNTs caused insufficient interparticle connection, whereas the lack of SWCNTs led to poor coverage of the entire surface of the NCM523 secondary particles. Both the conditions resulted in insufficient network formation from the perspective of electrical conduction. Based on these new findings, we assume that an appropriate combination of hybridization of MWCNTs and SWCNTs would promote continuous electrical conduction between each primary and secondary NCM523 particles, thereby enabling rapid electron transfer. Short MWCNTs were found to stabilize the electron conduction network three-

dimensionally through self-assembly at the grain boundaries formed by the primary NCM523 particles and the intergranular spaces formed at the neighbouring secondary NCM523 particles. Besides, the long and highly electron-conductive SWCNTs were found to mainly cover the surface of the secondary particles, thereby forming robust electron conduction pathways at the particle surface and over the adjacent particles. Since these equilibria are sensitive to the mixing ratio of each type of CNTs, they can be said to be one of the reasons for narrowing the process window to achieve higher performances.

3.3 Cycling stability of NCM/SW electrodes

The effects of the 3D network on the cycling stability of the half-cells were evaluated by a series of galvanostatic charge–discharge tests performed at a current density of 1 C (Fig. 3a). All the electrodes exhibited a similar initial discharge capacity of ca. 150 mAh/g, independent of the SWCNT contribution. 995NCM/SW0 showed significant capacity degradation from an early stage of the cycles (within 25 cycles), and the discharge capacity reached 18 mAh/g eventually. In contrast, the hybridized CNT networks delayed the number of cycles at which sudden specific capacity degradation occurred to 160 (995NCM/SW15), 180 (995NCM/SW10), and 190 cycles (99NCM/SW0). Note that such rapid capacity fading was not observed in the 995NCM/SW12 cell. Moreover, side reactions occurred at the interface of the cathode and electrolyte, which are triggered by the decomposition of electrolyte, and are one of the most powerful contributors to capacity degradation during cycling.[28–30] It is considered that unstable 3D-network formation within the electrode triggered side reactions at the electrode/electrolyte interfaces, leading to sudden capacity loss. Microcrack formation in an individual particle, frequently appeared in NCM-based secondary particle systems during cycling with deep charge-discharge level, offered the disconnection of electron conducting path, leading to reduce the rate of utilizing active materials. Furthermore, the microcrack promotes the side reactions due to the increase of surface area which contacts with electrolyte. Infiltrated electrolyte contacting with newly developed surface results in the severe capacity fading. To clarify this hypothesis, we introduced vinylene carbonate (VC) as additives for mitigating the influence of electrolyte deformation during long cycles at anode side. 995NCM/SW0 and 995NCM/SW12 electrodes were constructed full cell with graphite anode (Figure 3b). Although 995NCM/SW0-based full-cell presented gradual decline at early stage of cycling, as compared with the half-cell without additives, it still showed significant capacity degradation from around the 80th cycle. In contrast, 995NCM/SW12 exhibited higher capacity retention of >94% with a coulombic efficiency of >99.5% after 300 cycles. Therefore, these results demonstrate that appropriate combination of MW- and SW-CNTs not only contribute to electrochemical performance, but also improve structural stability.

As shown in Fig. 3c, the surface FE-SEM image of the 300th cycled 995NCM/SW0 electrode suggests that an appropriate hybridization condition of MWCNTs and SWCNTs increased the structural robustness of the extremely highly loaded NCM523 electrode, which strongly contributed to the cyclability improvement. The 3D networks of the NCM523 secondary particles in the 995NCM/SW0 electrode intensely collapsed at the grain boundaries and fractured into primary particles, resulting in the disconnection of electrical networks in the electrodes. In contrast, hybridization hindered the formation of intergranular cracks in the 3D network structures in the 995NCM/SW12 electrode. The secondary particles with densely packed electrode surface were stable after 300 cycles. The hybridized CNT network tightly held and connected each primary and secondary particle (Fig. 3d, e).

In addition, the collapse of the 3D network in the binder-free electrodes was found to accelerate the phase transition from a layered rock salt structure to a tetragonal phase. As shown in the X-ray diffraction (XRD) profiles after 300 cycles (Fig. 3f), the integrated $I_{(003)}/I_{(104)}$ intensity ratios of 995NCM/SW0 and 995NCM/SW12 are 0.86 and 1.19, respectively, which indicate less cation mixing with Li^+ and transition metal ions as well as the phase transition in 995NCM/SW12.[31,32] The disconnection of the electrically conducting CNT network associated with the collapse of the NCM523 secondary particles would promote inhomogeneous electrochemical reaction in the electrodes, leading to a disproportional reaction and subsequent phase transition of the NCM523 crystal in addition to the side reactions at the NCM523 particle surface, including the unexpected excess SEI formation and dissolution of transition metals into the electrolyte. Therefore, these experimental evidences strongly suggest that an appropriate SWCNT content play a key role in the formation of a robust 3D network system and the associated positive effects in battery performances. We prepared all the electrodes demonstrated here by using same parameters to exclude influence of other factors. Since carbon materials exhibit low density, small difference in weight concentration provides huge difference in number of CNTs. Furthermore, SW and MW have a different primary function. MW-CNT were consumed primary for connecting the interparticle and took the central role in the electron conducting path at interparticle, in contrast SW-CNT contributed the NCM particle surface electron conducting via particle surface coating.

3.4 Electrochemical performance of NCA/SW electrodes

We applied the hybrid 3D CNT network system to a $LiNi_{0.82}Co_{0.15}Al_{0.03}O_2$ (NCA) cathode, which has emerged as one of the most attractive high-capacity cathode material candidates. The NCA/CNT electrodes were composed of 99 wt% NCA and 1 wt% of the CNT hybrid. The amount of SWCNT in the CNT hybrid was controlled between 0, 5, 7 and 10 wt%. The microstructure of NCA/CNT electrodes show that an introduction of SWCNTs contributed the 3D network structure formation with good coverage given 1 wt% of CNTs (Fig. S4). As shown in Fig. 4a, the C-rate capabilities showed similar trends for the series of NCM/CNT electrodes reported in this paper. All the electrodes presented a discharge capacity of approximately 193 mAh/g regardless of the SWCNT content at a lower current

density (0.2 C). In contrast, the absence of SWCNTs resulted in significant capacity degradation as a function of current density. Moreover, in the cycling stability test (Fig. 4b), 99NCA/SW0 exhibited drastic capacity degradation from the 115th cycle, whereas 99NCA/SW5, 99NCA/SW7, and 99NCA/SW10 showed significantly less capacity degradation. A different tendency with NCM/SWs may arise from acceptable interparticle disconnecting given CNTs amount.

Further investigation on the cyclability was performed constructing full cells with VC additives (Fig 4c). Although 99NCA/SW0 full cell did not shows sudden capacity loss, as compare with 99NCA/SW0 without additives due to reduced electrolyte decomposition. It showed linear capacity decline, whereas 99NCA/SW5 presented better capacity retention (90 %) with a coulombic efficiency (99.5 %). Both of electrodes did not show significantly morphological changes in the secondary particles, as appeared in the 995NCM/SW0 electrodes (Fig. S5). However, partial fragmentation of the individual NCM secondary particles due to absence of SWCNTs in the 99NCA/SW0 was observed in the cycled electrodes, and which might contribute capacity fading.

Based on the above results, the use of the hybrid 3D-CNT networks system led to an efficient charge/discharge reaction for NCA, whereupon which showed high C rate capability with capacities of >130 $mAh{\cdot}g^{-1}$ at 10C only using 1 wt% of conductive agents, a value of that taken in extremely-loaded NCA electrode is comparable to literature that achieved in other systems, such as conjugated polymers and MWCNTs with less loadings.[9,16,33–35]

4. Conclusions

An extremely high-loading NCM523 and NCA cathode was achieved through the self-organization of a homogeneous 3D network structure. The hybridization of major MWCNTs with a small amount of minor SWCNTs with an appropriate composition resulted in superior C-rate capability (105 mAh/g at 10 C) and long cycling stability (94% capacity retention after 300 cycles) without the need of any polymeric binder. Systematic studies were conducted to determine the formation mechanism and structural characteristics of the hybridized 3D networks. The shorter MWCNTs spontaneously incorporated into the intergranular nanospaces, which promoted the interparticle bridging, while the longer SWCNTs homogeneously covered the entire surface of the particles. The 3D grid structures demonstrated here could provide enough electron conductivity and Li^+ accessibility as well as structural stability. Moreover, it is applicable to double-sided coating of an Al current collector, which shows high flexibility for mass production since the 3D network system can be prepared using the conventional slurry coating. Therefore, the proposed strategy could be an alternative and effective way for enhancing the energy density while maintaining a high C-rate capability and cyclability of Li-ion batteries for EV applications which have a range of 500 Km/Charge.

Acknowledgement

This work was partially supported by JST-CREST Grant Number JPMJCR1322 JAPAN. N. Z. acknowledges JSPS KAKENHI Grant Number 17H01322.

Notes and references

1 Z. P. Cano, D. Banham, S. Ye, A. Hintennach, J. Lu, M. Fowler, Z. Chen, *Nat. Energy*, **3**, 279–289.
2 M. A. Hannan, M. S. H. Lipu, A. Hussain and A. Mohamed, *Renew. Sust. Energ. Rev.*, 2017, **78**, 834–854.
3 N. Alias and A. A. Mohamad, *J. Power Sources*, 2015, **274**, 237–251.
4 A. Farmann, W. Waag, A. Marongiu and D. U. Sauer, *J. Power Sources*, 2015, **281**, 114–130.
5 X. Feng, M. Ouyang, X. Liu, L. Lu, Y. Xia and X. He, *Energy Storage Materials*, 2018, **10**, 246–267.
6 J. Jaguemont, L. Boulon and Y. Dubé, *Applied Energy*, 2016, **164**, 99–114.
7 Q. Wang, B. Jiang, B. Li and Y. Yan, *Renew. Sust. Energ. Rev.*, 2016, **64**, 106–128.
8 C. Zhan, T. Wu, J. Lu and K. Amine, *Energy Environ. Sci.*, 2018, **11**, 243–257.
9 J. H. Lee, C. S. Yoon, J.-Y. Hwang, S.-J. Kim, F. Maglia, P. Lamp, S. T. Myung and Y. K. Sun, *Energy Environ. Sci.*, 2016, **9**, 2152–2158.
10 U.-H. Kim, S. T. Myung, C. S. Yoon and Y. K. Sun, *ACS Energy Lett.*, 2017, **2**, 1848–1854.
11 J. Lee, J. K. Papp, R. J. Clément, S. Sallis, D.-H. Kwon, T. Shi, W. Yang, B. D. McCloskey and G. Ceder, *Nat. Commun.*, 2017, **8**, 981.
12 K. J. Park, M. J. Choi, F. Maglia, S.-J. Kim, K. H. Kim, C. S. Yoon and Y. K. Sun, *Adv. Energy Mater.*, 2018, **8**, 1703612.
13 M. Xu, L. Fei, W. Zhang, T. Li, W. Lu, N. Zhang, Y. Lai, Z. Zhang, J. Fang, K. Zhang, J. Li and H. Huang, *Nano Lett.*, 2017, **17**, 1670–1677.
14 S. Kuwabata, S. Masui and H. Yoneyama, *Electrochim. Acta*, 1999, **44**, 4593–4600.
15 H. Wang, Y. Zeng, K. Huang, S. Liu and L. Chen, *Electrochim. Acta*, 2007, **52**, 5102–5107.
16 C.-H. Lai, D. S. Ashby, T. C. Lin, J. Lau, A. Dawson, S. H. Tolbert and B. S. Dunn, *Chem. Mater.*, 2018, **30**, 2589–2599.
17 O. Toprakci, H. A. K. Toprakci, L. Ji, G. Xu, Z. Lin and X. Zhang, *ACS Appl. Mater. Interfaces*, 2012, **4**, 1273–1280.
18 C. Ban, Z. li, Z. Wu, M. J. Kirkham, Le Chen, Y. S. Jung, E. A. Payzant, Y. Yan, M. S. Whittingham and A. C. Dillon, *Adv. Energy Mater.*, 2011, **1**, 58–62.
19 S. Luo, K. Wang, J. Wang, K. Jiang, Q. Li and S. Fan, *Adv. Mater.*, 2012, **24**, 2294–2298.
20 D.-W. Kim, N. Zettsu and K. Teshima, *J. Mater. Chem. A*, 2017, **5**, 22797–22804.
21 J.-H. Shim, Y.-M. Kim, M. Park, J. Kim and S. Lee, *ACS Appl. Mater. Interfaces*, 2017, **9**, 18720–18729.
22 L. Wang, D. Mu, B. Wu, G. Yang, L. Gai, Q. Liu, Y. Fan, Y. Peng and F. Wu, *Electrochim. Acta*, 2016, **222**, 806–813.
23 J.-Z. Kong, C. Ren, G.-A. Tai, X. Zhang, A.-D. Li, D. Wu, H. Li and F. Zhou, *J. Power Sources*, 2014, **266**, 433–439.
24 J. Kang, H. Q. Pham, D.-H. Kang, H.-Y. Park and S.-W. Song, *J. Alloy. Compd.*, 2016, **657**, 464–471.
25 J. Xie, A. D. Sendek, E. D. Cubuk, X. Zhang, Z. Lu, Y. Gong, T. Wu, F. Shi, W. Liu, E. J. Reed and Y. Cui, *ACS Nano*, 2017, **11**, 7019–7027.
26 C. J. Jafta, M. K. Mathe, N. Manyala, W. D. Roos and K. I. Ozoemena, *ACS Appl. Mater. Interfaces*, 2013, **5**, 7592–7598.
27 Z. Wu, X. Han, J. Zheng, Y. Wei, R. Qiao, F. Shen, J. Dai, L. Hu,

K. Xu, Y. Lin, W. Yang and F. Pan, *Nano Lett.*, 2014, **14**, 4700–4706.
28 J. Xia, M. Nie, J. C. Burns, A. Xiao, W. M. Lamanna and J. R. Dahn, *J. Power Sources*, 2016, **307**, 340–350.
29 J. Xia, K. J. Nelson, Z. Lu and J. R. Dahn, *J. Power Sources*, 2016, **329**, 387–397
30 J. Xia and J. R. Dahn, *J. Power Sources*, 2016, **324**, 704–711.
31 J. Ying, C. Wan, C. Jiang and Y. Li, *J. Power Sources*, 2001, **99**, 78–84.
32 Y. Kim, *ACS Appl. Mater. Interfaces*, 2012, **4**, 2329–2333.
33 L. Zhang, J. Fu and C. Zhang, *Nanoscale Res. Lett.*, 2017, **12**, 376.
34 S. Xia, F. Li, F. Chen and H. Guo, *J. Alloy. Compd.*, 2018, **731**, 428–436.
35 M. Jo, M. Noh, P. Oh, Y. Kim and J. Cho, *Adv. Energy Mater.*, 2014, **4**, 1301583.

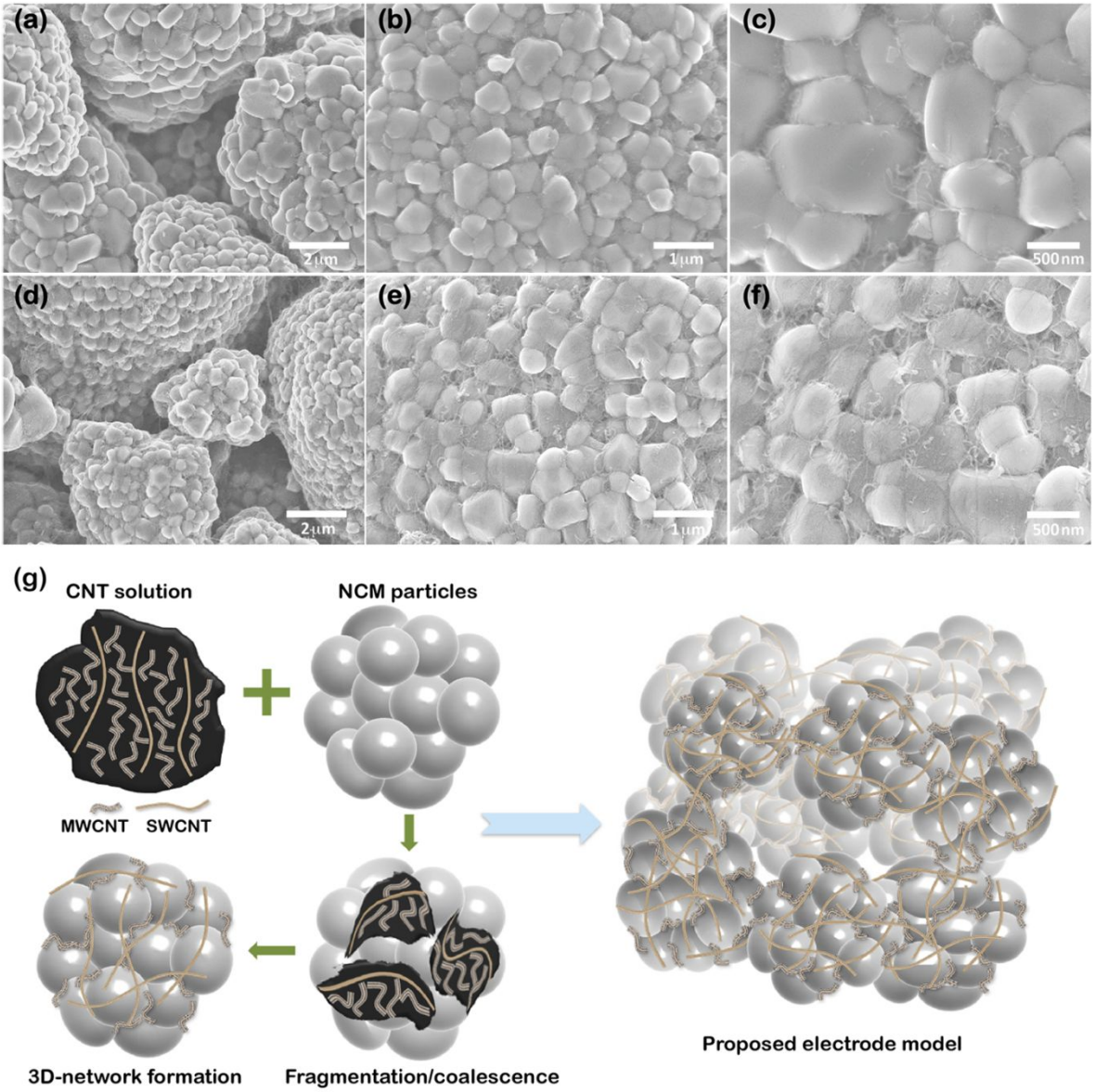

Fig. 1 FE-SEM images of NCM/SW electrodes at different magnifications. (a–c) 995NCM/SW0 electrode and (d–f) 995NCM/SW12 electrode. (g) Schematic illustration of 3D-network formation mechanism and proposed electrode model.

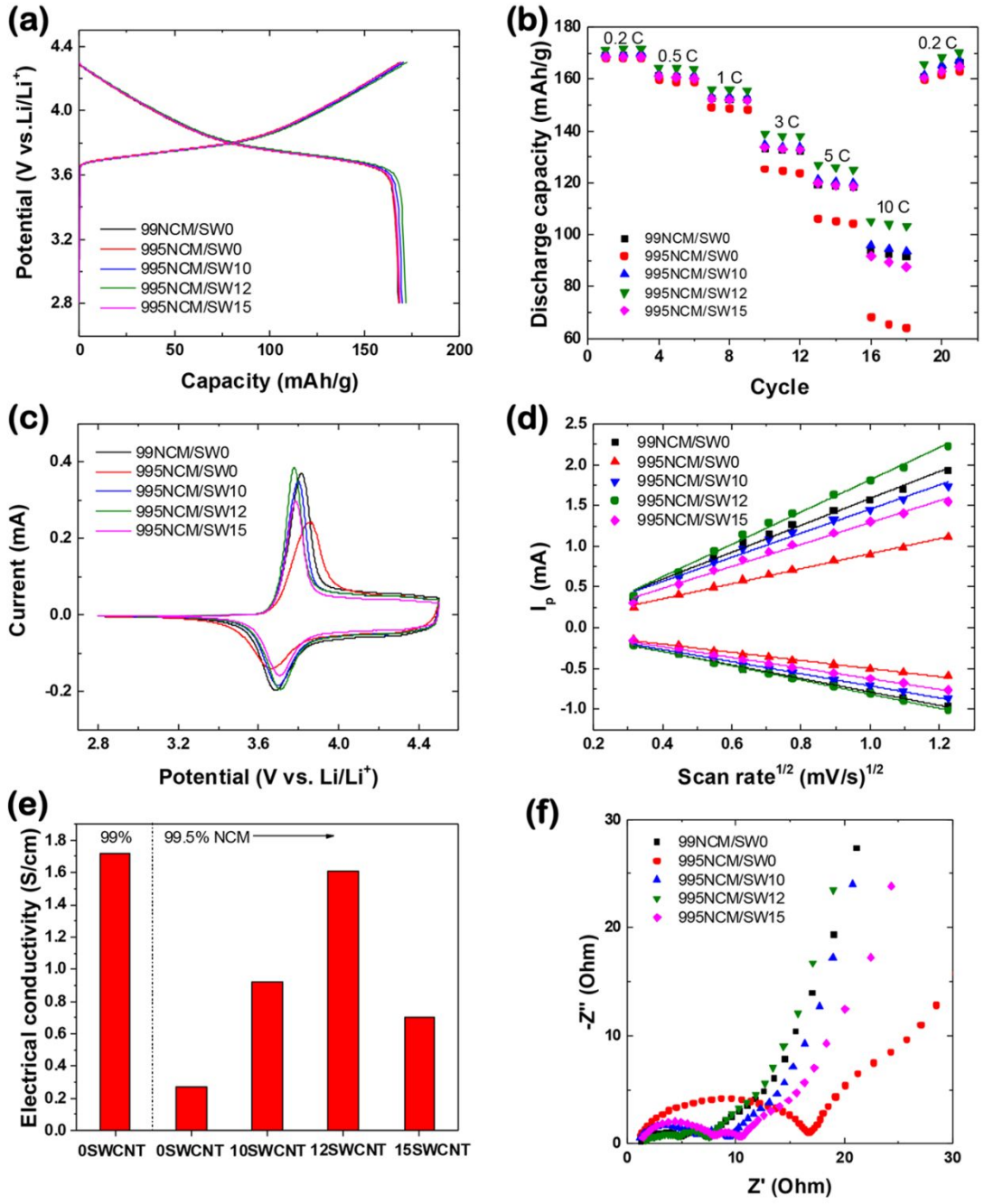

Fig. 2 Electrochemical properties of NCM/SW electrodes. (a) Charge–discharge profiles at current density of 0.2 C for 3rd cycle. (b) C-rate capability at various current densities from 0.2 to 10 C. (c) Cyclic voltammetry profiles in the potential range of 2.8–4.5 V at scan rate of 0.1 mV/s. (d) Linear response of peak current density as a function of square root of scan rate. (e) Electrical conductivity of NCM/SW electrodes. f) Electrochemical impedance spectroscopy spectra.

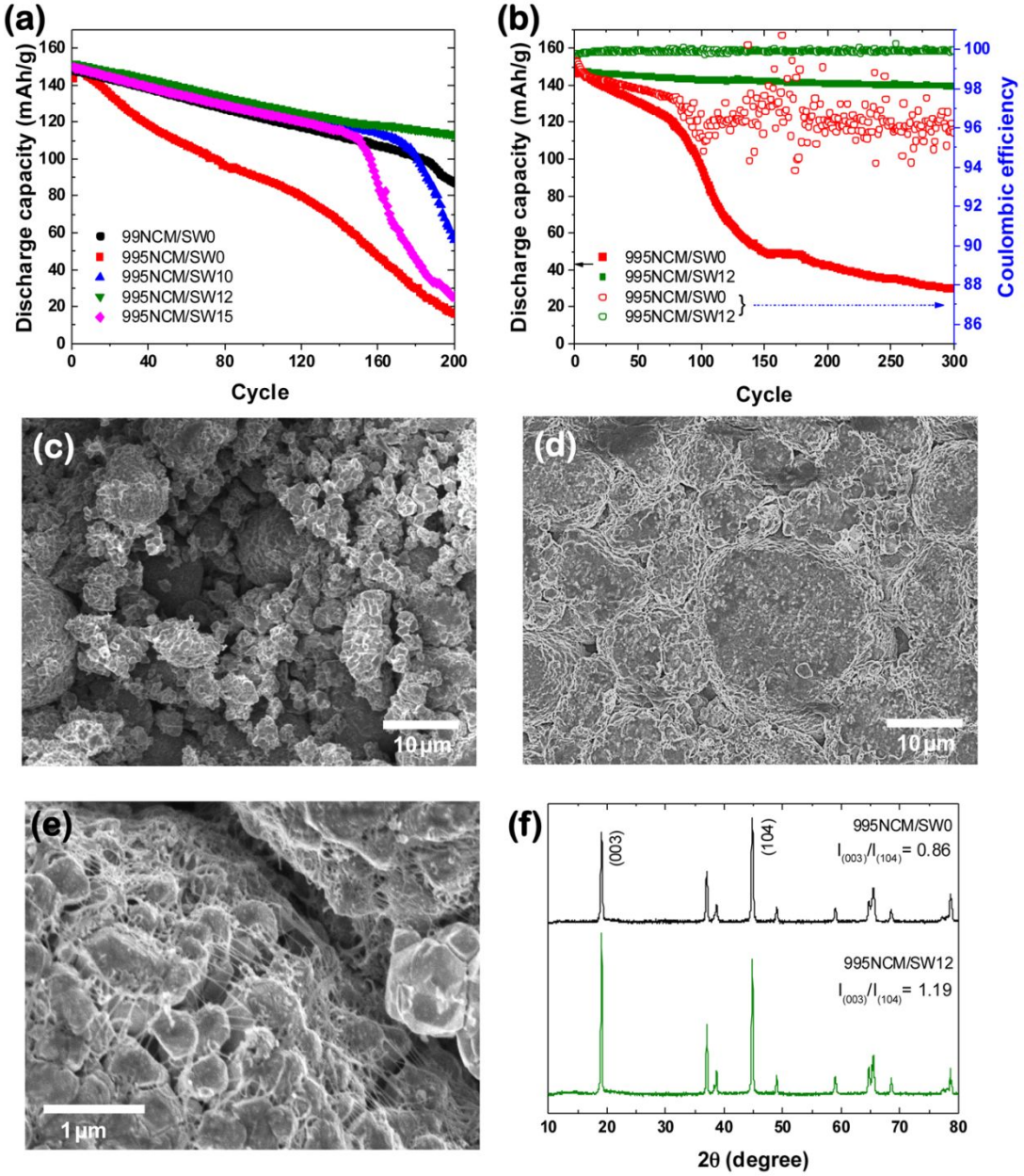

Fig. 3 Impact of 3D network structure on cycling performance. Cycling performance of (a) NCM/SW-Li half-cell at current density of 1 C for 200 cycles, and (b) 995NCM/SW0- and 995NCM/SW12-graphite full-cell with 0.5 wt% of VC at current density of 1 C for 300 cycles. SEM images of cycled cathode surface of (c) 995NCM/SW0 and (d, e) 995NCM/SW12. (f) XRD patterns of cycled 995NCM/SW0 and 995NCM/SW12 cathodes. 995NCM/SW0 with unstable 3D-network promotes disproportional reactions and unexpected side reactions, including O_2 release form NCM lattice with *R-3m* symmetry. It is leading to phase transition from layered rock-salt to tetragonal phase via the formation of vacancies of Li^+ and O^{2-} in $LiNiO_2$-grain. Ni^{2+} easily diffuses into vacant Li sites, resulting in increase of irregular arrangement of cations.

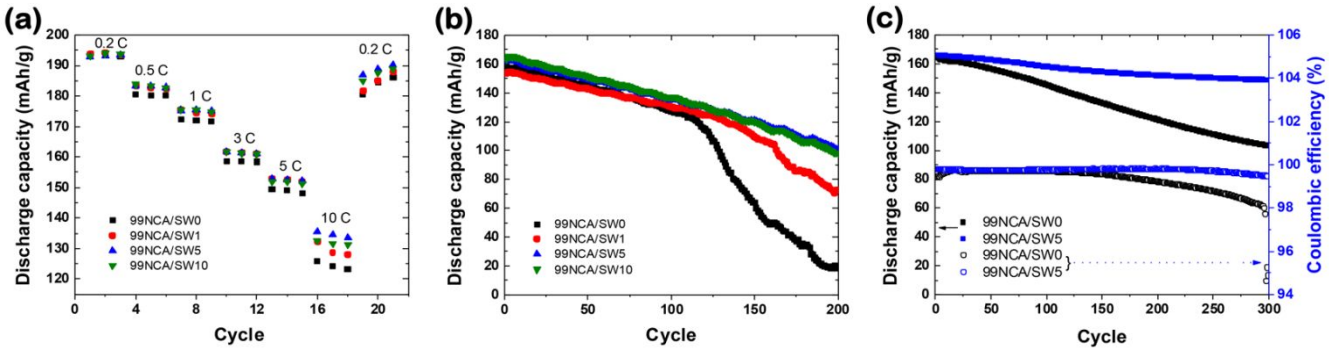

Fig. 4 Effect of hybrid 3D network structure of NCA electrodes. (a) C-rate capability at various current densities from 0.2 to 10 C. Cycling performance of (b) NCA/SW-Li half-cell at current density of 1 C for 200 cycles, and (c) 99NCA/SW0- and 99NCA/SW5-graphite full-cell with 0.5 wt% of VC at current density of 1 C for 300 cycles.